Modelling Wettability Alteration in Microporous Carbonate Rocks

W. Kallel[1], M.I.J. van Dijke[1], K.S. Sorbie[1], Z. Jiang[1], S. Harland[2], R. Wood[2]

1. Institute of Petroleum Engineering, Heriot-Watt University, Riccarton, Edinburgh, EH14 4AS, United Kingdom.
2. School of GeoSciences, University of Edinburgh, West Mains Road, Edinburgh, EH9 3JW, United Kingdom.

Abstract:

Carbonate-hosted hydrocarbon reservoirs are known to be weakly- to moderately oil-wet, but the pore-scale wettability distribution is poorly understood. Moreover, micropores, which often dominate in carbonate reservoirs, are usually assumed to be water-wet and their role in multi-phase flow is neglected. Modelling the wettability of carbonates using pore network models is challenging, because of our inability to attribute appropriate chemical characteristics to the pore surfaces and over-simplification of the pore shapes. Here, we implement a qualitatively plausible wettability alteration *scenario* in a two-phase flow network model that captures a diversity of pore shapes. The model qualitatively reproduces patterns of wettability alteration recently observed in microporous carbonates via high-resolution imaging. To assess the combined importance of pore-space structure and wettability on petrophysical properties, we consider a homogeneous Berea sandstone network and a heterogeneous microporous carbonate network, whose disconnected coarse-scale pores are connected through a sub-network of fine-scale pores. Results demonstrate that wettability effects are significantly more profound in the carbonate network, as the wettability state of the micropores controls the oil recovery.

Keywords: Network Modelling; Two-phase flow; Carbonates; Microporosity; Wettability Alteration.

1. Introduction

Understanding the wettability state of a porous medium is essential for accurate modelling of multi-phase flow processes in hydrocarbon reservoirs, as well as in aquifers following contamination by non-aqueous phase liquids or injection of carbon-dioxide. Specifically in simulations of hydrocarbon reservoir behaviour, assumptions on the wettability distribution strongly influence many petrophysical functions. This includes the capillary pressure and relative permeability data, as well as the oil recovery efficiency after waterflooding (**Salathiel 1973; Jadhunandan and Morrow 1995**). The stakes become notably important when dealing with carbonate rocks, as such formations host more than 60% of the World's remaining oil reserves and the recovery efficiency from carbonate reservoirs is often considered to be low.

To evaluate the average wettability of reservoir core samples, indirect methods requiring capillary pressure data are used, including Amott (**Amott 1959**), USBM (United States Bureau of Mines) (**Donaldson et al., 1969**) and Amott/USBM combined method (**Sharma and Wunderlich 1987**). Many studies using these tests confirm that carbonate rocks show intermediate to weakly oil-

wet behaviour at the core scale (**Lichaa et al., 1993; Al-Yousef et al., 1995; Skauge et al., 2007**; **Okasha et al., 2007**).

No universal procedure is, however, currently available to assess how wettability is distributed on a pore by pore basis in reservoir rocks, but wettability is known to be heterogeneous at the pore scale (**Fassi-Fihri et al., 1995)**. Particularly, the wetting state of micropores, defined here where pores <5 μm in radius **(Cantrell and Hagerty 1999)**, is of particular interest; as such porosity can account for up to 100% of the total porosity in carbonate reservoirs **(Cantrell and Hagerty, 1999).** Micropores wettability has been largely unknown or they are assumed to be water-wet, in contrast to oil-wet macropores (**Fassi-Fihri et al., 1995)**. This shouldn't be a rule as oil has actually been detected within micropores in several real carbonate reservoirs (**Al-Yousef et al., 1995; Clerke, 2009; Knackstedt et al., 2011; Fung et al., 2011; Clerke et al., 2014; Dodd et al., 2014),** which may alter their wettability.

Qualitatively, imaging techniques are able to reveal wettability distributions in rocks at the level of individual pores. For example, using Cryo-SEM imaging technique, **Fassi-Fihri et al. (1995)** examined a Middle Eastern carbonate reservoir and observed that micropores were water-wet, in contrast to oil-wet mesopores. More recently, higher resolution Field-Emission SEM (FESEM) imaging identified the existence of a pattern of wettability alteration within micropores in reservoir carbonates according to **Knackstedt et al. (2011)**, **Marathe et al. (2012)** and **Dodd et al. (2014).** They suggested that the wettability alteration on calcite microrhombs is face-selective, where the anhedral ("curved, rough and poorly formed") faces are preferentially oil-wet, as opposed to the euhedral ("flat, smooth, well-formed") which remained water-wet. These techniques are however limited, as they are unable to capture the full heterogeneity of the rock wettability distribution.

Wettability is thought to be dependent on several factors. Indeed, **Fassi-Fihri et al. (1995)** observed that wettability in carbonates was mostly affected by pore geometry, while mineralogy was found to be the major factor controlling wettability in sandstones. On the other hand, **Hamon (2000)** examined a dataset from a sandstone hydrocarbon reservoir and found no evidence that pore mineralogy has any direct impact on wettability.

From a theoretical perspective, Pore Network Modelling has proved to be an efficient tool to study the effect of wettability at the macroscopic scale, especially on oil recovery (**McDougall and Sorbie 1995**; **McDougall et al., 1997; Blunt 1997a, 1997b; Blunt 1998; Dixit et al., 1999**; **Zhao et al., 2010**; **Ryazanov et al., 2014**). **McDougall and Sorbie (1995)** proposed a classification system for mixed-wettability states, where wettability is either distributed according to pore size: Mixed-Wet Large (MWL) and Mixed-Wet Small (MWS), where large and small pores respectively are oil-wet, or uncorrelated to pore size: Fractionally-Wet (FW). Using pore scale modelling, the consequences of these wettability distributions on the observed wettability indices (both USBM and Amott) were predicted by **Dixit et al. (2000)**. Experimental evidence has since confirmed that MWL, MWS and FW distributions can all be observed in real reservoir cores (**Skauge et al., 2007)**. Specifically, **Skauge et al. (2006)** examined a broad (mostly microporous) carbonate dataset and found that following a core-flooding and aging procedure, nearly all the samples exhibited MWS behaviour according to the combined Amott/USBM test, which is contrary to the common assumptions. In fact, these theoretical wettability distributions, although helpful to study simple cases, may be insufficient to describe complex wettability distributions, especially in microporous carbonates.

Kovscek et al. (1993) established a pore-level scenario to describe the mixed wettability development in reservoirs, based on the concept of thin films coating the pore wall, which preserve its initial wettability state during ageing. In this scenario wettability is controlled by the stability of the thin film, which in turn depends on the fluid system, the mineralogy of the rock surface, the local pore geometry, and the prevailing capillary pressure. They incorporated this scenario in a capillary bundle model with star-shaped pore cross sections. The resulting capillary pressure curves, residual oil saturations and Amott-Harvey indices showed reasonable qualitative agreement with experimental results. **Frette et al. (2009)** incorporated this scenario in a bundle-of-tubes theoretical model with 2D realistic pore cross sections derived from high resolution SEM images, for which they examined the relationship between collapsed films fraction and capillary pressure. The scenario has also been implemented in 3D network models (**Blunt 1997b,1998**; **Oren et al., 1998**; **Jackson et al., 2003**). To allow wettability changes to occur, these models employed angular pore cross sections, and a simple parametric model for the water film collapse.

In the current work, we implemented the **Kovscek et al. (1993)** scenario in a two-phase flow network model that takes into account a variety of pore shapes (**Ryazanov et al., 2009, 2014**), more representative of the complexity of real carbonate rocks. Equivalent pore wall curvatures are assigned based on pore size and shape. Moreover, the disjoining pressure is inferred from the fraction of oil-wet pores and the maximum achieved capillary pressure. In Section 2 we present this network modelling tool and describe the flooding cycle of primary drainage, wettability alteration and subsequent water invasion. In Section 3 we investigate the role of the wettability distribution on oil recovery for pore space structures of different complexities, starting with a relatively simple network taken from a Berea sandstone core, which is then compared with a multiscale network derived from a complex, microporous carbonate rock. For the carbonate case, we further examine the importance of the wettability state of the micropores for oil recovery.

2. Model description

The two-phase flow pore network modelling tool used in this study is similar to the models developed by **Oren et al. (1998**), **Patzek (2001**), **Valvatne and Blunt (2004**). It has been thoroughly described by **Ryazanov et al. (2009,2014)**. It requires as input networks consisting of pore bodies (nodes) interconnected via straight tubular pore throats (bonds). Networks are either generated numerically or extracted from 3D images of real pore spaces. The latter are topologically and geometrically equivalent representations of the porous media, preserving its connectivity and characteristic pore properties (inscribed and hydraulic radii, shape factor, volume, etc.). The shape of the pore cross-section is important for conductance and capillary entry pressure computations. This is usually characterised using the shape factor, to idealise it as a Circle, Triangle or Square (the CTS approach). The shape factor is defined as $G = {A}/{L^2}$, where A and L are the area and perimeter of the cross section, respectively. In the current model, in addition to the shape factor, we use the dimensionless hydraulic radius (if available) to idealise the pore shape as regular n-cornered stars, along with the CTS (**Helland et al., 2008**; **Ryazanov et al., 2009, 2014**).

The porosity of the network is estimated using the total volume of pores and throats relative to the volume of the enclosing domain. Both absolute and relative permeabilities are computed based on the total flow through the network for the phase cluster of interest, for a given applied pressure gradient and application of Darcy's law.

The network modelling tool is a quasi-static two-phase flow model. The capillary-driven flow is simulated using a classical Invasion Percolation (IP) process with trapping. We simulate the commonly used flooding cycle: primary drainage, ageing and water invasion, which mimics the flooding process undergone by a real hydrocarbon reservoir. First, primary drainage (PD) is simulated in a network initially saturated with water and water-wet (contact angle $\theta_{pd} \in [0,90°[$). The process of oil invasion may continue until the irreducible water saturation is reached where no further pore-scale displacements are possible under capillary controlled processes, or stopped at a fixed initial water saturation, S_{wi}, related to a predefined maximum capillary pressure, P_c^{max}. Subsequently, the model allows for wettability alteration of the oil-filled pore space due to ageing. Along with the commonly used wettability alteration scenarios, leading to the mixed-wet large (MWL), mixed-wet small (MWS) and fractionally-wet (FW) distributions, we have implemented a physically based wettability alteration scenario (Section 2.1), leading to the so-called AW distribution. Then, water invasion is simulated until the residual oil saturation, S_{or}, is reached, below which no further oil mobilisation can take place by capillary forces. Note that the model involves wetting films and layers in the pores with corners (Section 2.3).

2.1 Wettability alteration scenario

We model the physically-based wettability alteration scenario suggested by **Kovscek et al. (1993)**, illustrated in Figure 1, and refer to the resulting wettability distribution as Altered-Wet (AW). Initially, all pores are assumed to be filled with water and completely water-wet, and at this point we start injecting oil. As the water saturation decreases, thin water films coating the pore walls remain, which prevent the surface from contact with oil particles, hence preserving its strong initial affinity to water.

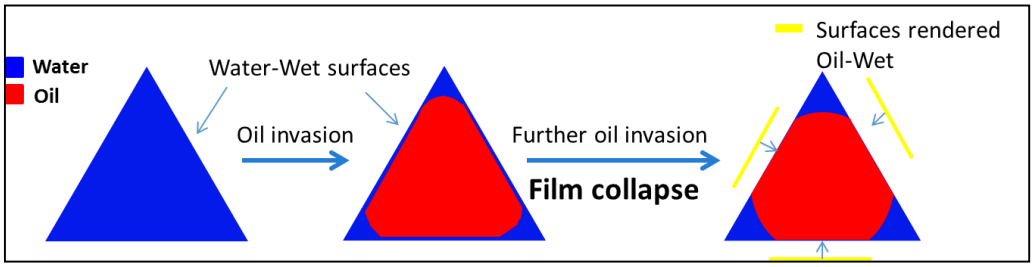

Figure 1: Illustration of the wettability alteration mechanism in a triangular pore cross-section.

At equilibrium, the water film in a given pore is stabilised by thin film forces; the related pressure is the so called disjoining pressure, Π. Three major factors contribute to the disjoining pressure: Electrostatic interactions, Van der Waals interactions and Hydration forces (**Hirasaki 1991**). As shown in the disjoining pressure isotherm (Figure 2), Π depends on the thickness of the water film. As the capillary pressure, $P_{c,}$ rises during oil invasion, the film gets thinner. The film first gains in stability since Π rises, until P_c reaches a threshold capillary pressure, P_c^*:

$$P_c^* = \Pi_{crit} + \sigma_{ow} c. \quad (1)$$

The threshold capillary pressure is an intrinsic property of the pore related to the oil-water interfacial tension, σ_{ow}, the curvature of the pore wall, c, and the critical disjoining pressure at which films collapse, Π_{crit}. In fact, when $P_c > P_c^*$, $i.e. \Pi < \Pi_{crit}$, the film becomes unstable and

breaks. Consequently, the pore surfaces adsorb compounds from the oil which may change their wetting state into oil-wet **(Kovscek et al., 1993)**.

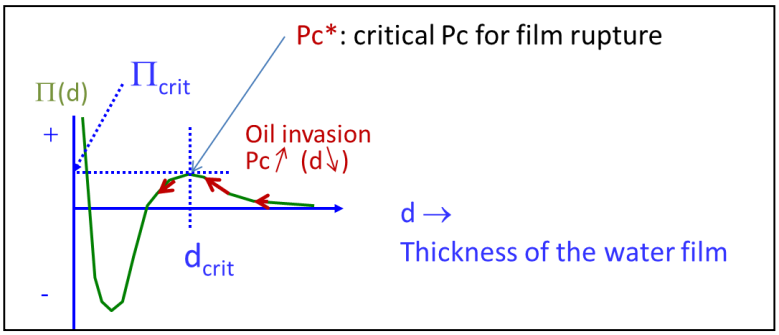

Figure 2: Evolution of thin film stability during oil invasion, illustrated on an example of disjoining pressure isotherm $\Pi(d)$*, after* (**Hirasaki 1991**).

In our pore network model, pore walls are represented by flat surfaces with zero curvature (regular polygon and star shapes), hence thin films would collapse simultaneously in all pores, as all P_c^* are equal for constant Π_{crit} (Equation 1). As it is difficult to obtain the real pore wall curvatures from a digitised image, we assign equivalent curvatures to the flat pore walls based on the overall pore shapes, for wettability alteration purposes only, as indicated in Figure 3. The curvature, $c = -\frac{1}{r_c}$, is assumed negative as the radius of curvature, r_c, is located outside the shapes. For regular polygons r_c is computed using Equation (2) (**Joekar-Niasar et al. 2010**), in which $\cos\varphi$ is randomly chosen. For regular stars r_c is computed from Equation (3). Note that while one random parameter ($\cos\varphi$) is introduced for polygons, the radius of curvature is fully determined for stars.

$$r_c^{n-polygon} = R_{ins}\frac{\sin\frac{\pi}{n}}{\cos\varphi-\sin\frac{\pi}{n}}, \qquad cos\varphi \in \left[sin\frac{\pi}{n}, 1\right] \tag{2}$$

$$r_c^{n-star} = R'_{ins}\frac{\sin\frac{\pi}{n}}{\cos\gamma-\sin\frac{\pi}{n}} = R_{ins}\frac{\sin\left(\gamma+\frac{\pi}{n}\right)sin\frac{\pi}{n}}{\sin\left(\gamma+\frac{\pi}{n}\right).\cos\gamma-\sin\frac{\pi}{n}}, \qquad \gamma\text{: corner half-angle} \tag{3}$$

where R_{ins} denotes the inscribed radius.

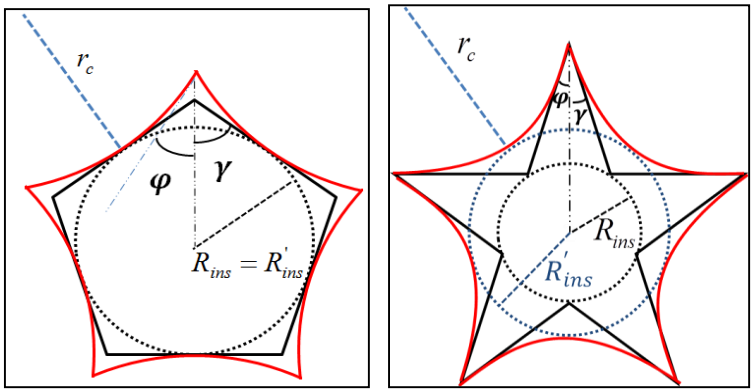

(a) (b)

Figure 3: Equivalent pore wall curvature assignment for (a) n-cornered Polygon and (b) n-cornered Star shape, where R_{ins} and R'_{ins} denote the original and new inscribed radii, respectively; r_c denotes the radius of curvature and φ the angle between the tangent to the newly obtained (red) curved shape at a vertex and the line connecting the vertex to the center (φ coincides with the corner half-angle, γ, for the original shapes).

According to Equation (1), by strictly using the negatively-curved star shapes introduced in Figure 3, the more curved the pore surface is (in absolute value), the more accessible (lower) is the capillary pressure at which the thin film collapses (P_c^*). Therefore, smaller pores of the same shape are more likely to be oil-wet. This is also the case for pores of the same size and shape but with a larger number of corners, which can be interpreted as corresponding to increased pore roughness. Therefore, the model qualitatively reproduces the pattern shown by high-resolution imaging in carbonate rocks (**Marathe et al. 2012**) where oil deposition on calcite microparticles was limited to the anhedral (curved, rough and poorly formed) faces (Figure 4).

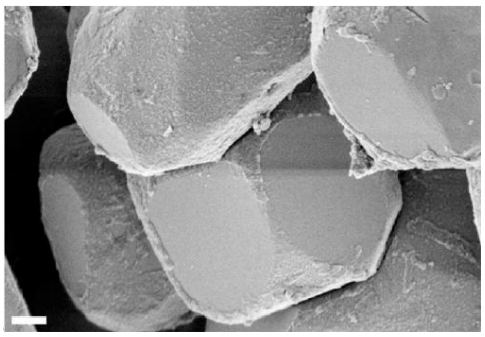

Figure 4: FESEM imaging of the oil deposits (i.e. the footprint of the wettability alteration) on calcite microparticles in carbonate rocks*, after* (**Marathe et al. 2012**).

Π_{crit} depends on the fluid system and mineralogy of the rock surface. We will assume in our model that it is constant throughout the rock, reflecting a mono-mineral carbonate. Π_{crit} is computed by the simulator, given a prescribed final drainage capillary pressure $P_c{}^{max}$ and a targeted volumetric oil-wet fraction (f_{ow}) of all pores. Note that a higher $P_c{}^{max}$ leads to a higher f_{ow}, as thinner films are more prone to collapse. On the other hand, higher Π_{crit} causes f_{ow} to decrease, since a higher P_c would need to be achieved to reach film rupture (at P_c^*). Below (Section 3.1.1,

3.2.2) we describe how this new AW distribution compares to previously described wettability distributions MWL, MWS and FW.

Since no comprehensive model is available for the distribution of the values of the advancing contact angle θ_a , these are assumed to be uniformly distributed within prescribed ranges in both the water-wet and oil-wet pores.

2.2. Oil layers formation and collapse

During waterflooding, oil layers may form in oil-wet pores, sandwiched between water in the centre and corners of the pores (**Ryazanov et al., 2009, 2014**) (Figure 5). The contribution of these layers to oil volume and flow is small compared to that of bulk fluid. Nevertheless, if stable, these layers play an important role in oil flow, as they preserve the oil phase connectivity. Formation and collapse of the layers occurs according to a realistic thermodynamic criterion (**van Dijke and Sorbie, 2006**).

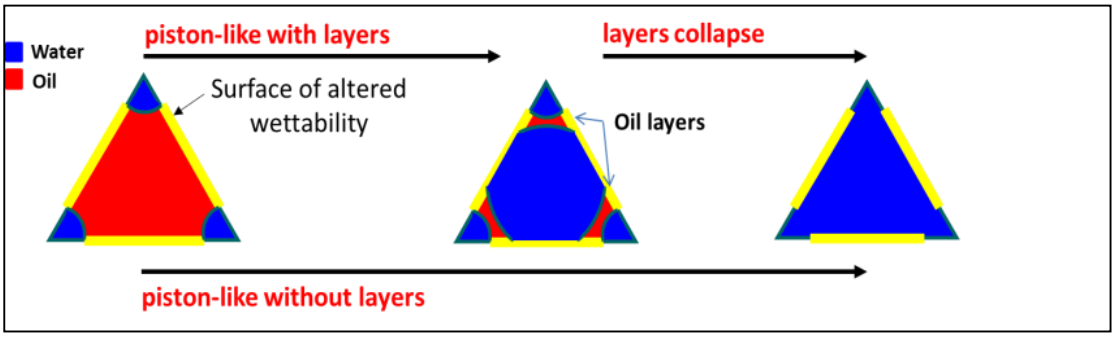

Figure 5: Displacements during waterflooding involving oil layers formation and collapse presented as transitions between fluid configurations in a triangular pore cross-section.

3. Results and discussion

The simulations are carried out on two distinctly different networks: a homogeneous sandstone network and a heterogeneous network derived from a microporous carbonate dataset (Jiang et al, 2013). The same "base case" is chosen for both networks (Table 1). At ageing, we uniformly distribute the water-wet and oil-wet advancing contact angles as $\theta_{a,ww}\epsilon[\theta_{pd}, 90°[$ and $\theta_{a,ow}\epsilon[120°, 180°]$, respectively. Note that the value of $\theta_{pd} = 30^0$ corresponds to an initially weakly water-wet rock.

S_{wi}	*0*
$\theta_{pd}(^o)$	*30*
f_{ow}	*0.5*
Wettability distribution	*AW*

Table 1: "Base case" parameters.

3.1. Berea Sandstone Network

The network (Figure 6a) has been extracted from a 3D micro-computed tomography image of a Berea sandstone sample, using the enhanced extraction technique described by **Jiang et al. (2007).** Its characteristics are summarized in Table 2. Figure 6b shows that the pore size distribution is unimodal, and that larger pores tend to have more corners.

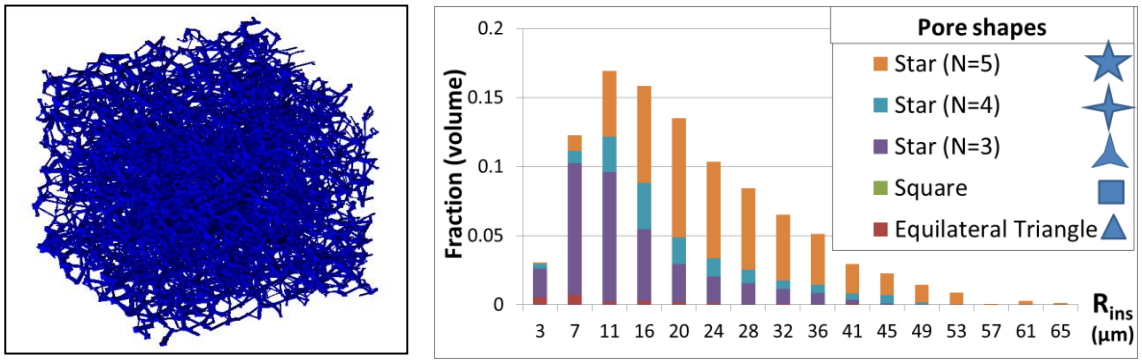

(a) (b)

Figure 6: Berea network: (a) 3D representation and (b) pore size (inscribed radius) and shape distributions.

Number of pore elements (nodes and bonds)	*22,251*
Average coordination number	*3.7*
Porosity (%):	*18.97*
Absolute Permeability (mD):	*1576.38*

Table 2: Main properties of the Berea network.

3.1.1 Primary Drainage

In the base case, the primary drainage (PD) process is continued until the irreducible water saturation is reached at $P_c{}^{max} = 22kPa$ (Figure 7). As shown in Figure 8, all invaded pores are sufficiently water-wet ($\theta_{pd} < \frac{\pi}{2} - \gamma$) to hold water in the corners, which forms the irreducible water saturation $S_{wi} < 0.01$. In a second case, oil invasion is stopped at prescribed initial water saturation $S_{wi} = 0.3$ ($P_c{}^{max} = 5kPa$). As expected, water is mainly left behind in the smallest pores, for which the capillary entry pressures are highest.

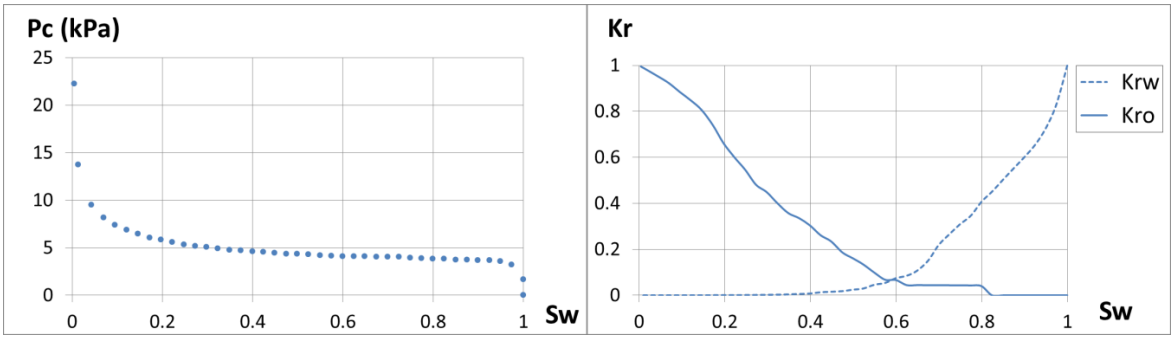

(a) (b)

Figure 7: Primary drainage (a) P_c and (b) K_r curves for the Berea network.

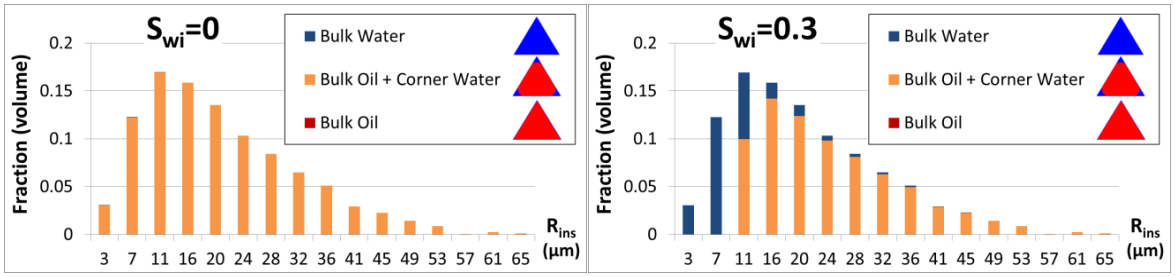

Figure 8: Pore occupancies for the Berea network shown on the pore size distribution following PD to different S_{wi} values.

3.1.2 Ageing

The different wettability distributions (MWL, MWS, FW and AW) resulting after PD are plotted in Figure 9 on the volumetric pore size distributions. In the MWL (resp. MWS) distribution, oil-wet pores are evidently the largest (resp. smallest). The FW distribution (at $f_{ow} = 0.5$) results in half the pores being oil-wet for each bin size. On the other hand, AW exhibits a more complex distribution, where both pore size and shape determine the wettability distribution. For instance, the size of the largest pores ($R_{ins} \geq 41\mu m$) prevents them from having sufficient curvature for the water film to break, thus leaving them water-wet. Moreover, few small pores are found to be oil-wet. Indeed, the smallest pores are mostly characterised by 3-cornered star shapes (Figure 6b), and as previously stated (Section 2.1), pores with smaller number of corners (reduced roughness) are less likely to be oil-wet.

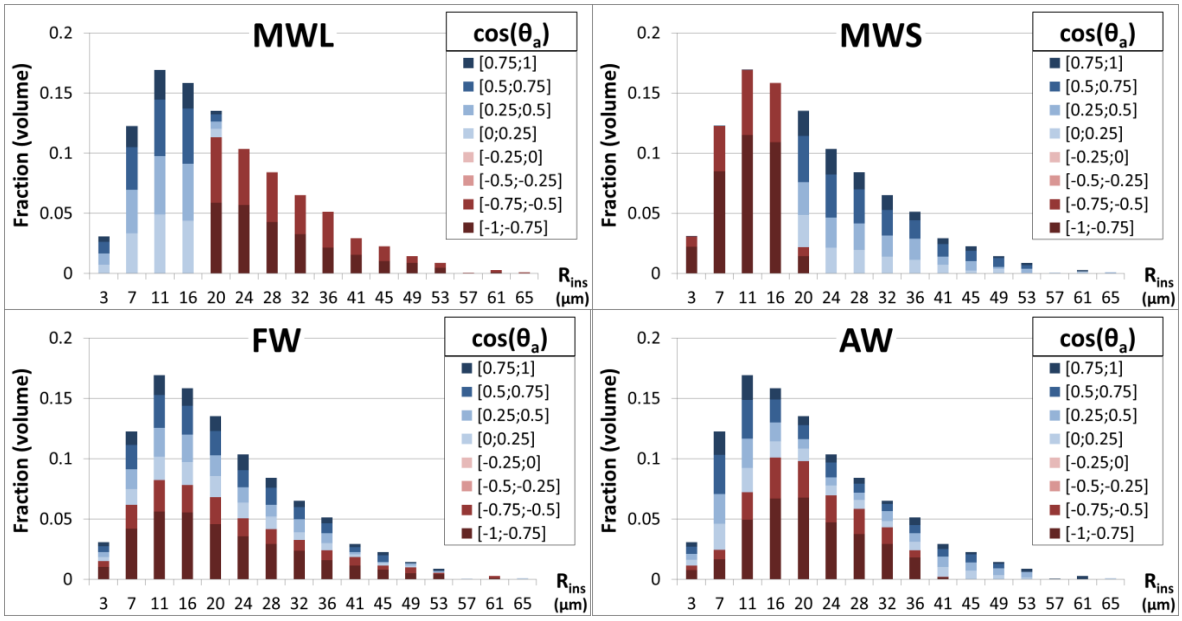

Figure 9: Different wettability distributions shown on the pore size distributions for the Berea network at $f_{ow} = 0.5$, established after PD for the base case; red: oil-wet, blue: water-wet. Darker blue (resp. red) indicates stronger water- (resp. oil) -wetness.

3.1.2 Waterflood

3.1.2.1 Effect of wettability distribution

The effect of varying the wettability distribution on the residual oil saturation, S_{or}, was found to be small (Figure 10a). This behaviour could be explained by the homogeneity of the sandstone structure, where pores are connected to one another regardless of size. We will show below that the effect of the wettability distributions on S_{or} is much more profound for the heterogeneous Carbonate network (Section 3.2.3, Figure 21a), whose topology is much more complex.

From the pore occupancies at $f_{ow} = 0.5$ (Figure 11) it is clear that the residual oil distribution is greatly affected by the wettability distribution. In all cases, we find that the residual oil is mostly present in oil-wet pores, as expected. A few oil layers formed near the end of the waterflood process, mainly in the largest oil-wet pores, whose layers formation entry pressure are highest. The effect of the presence of oil layers on S_{or} is shown for the AW distribution in Figure 10b. The "with layers" case corresponds to the base case where oil layers formation is enabled. On the contrary, the oil layers formation was disabled in the "no layers" case. As expected, oil layers allow oil to drain to lower S_{or} when f_{ow} is sufficiently large (for this rock $f_{ow} \geq 0.5$) for a spanning (percolating) oil-wet pathway to be formed.

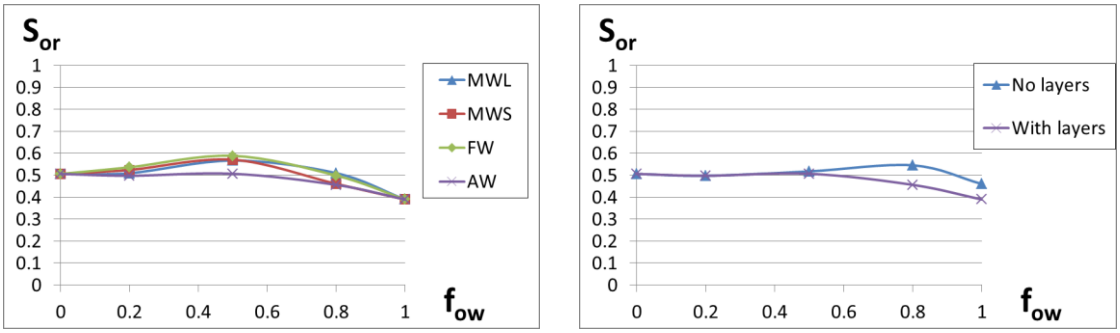

(a) (b)

Figure 10: Waterflood residual oil saturations as a function of oil-wet fractions for the Berea network (a) for the different wettability distributions, and (b) for the AW distribution, with and without oil layers.

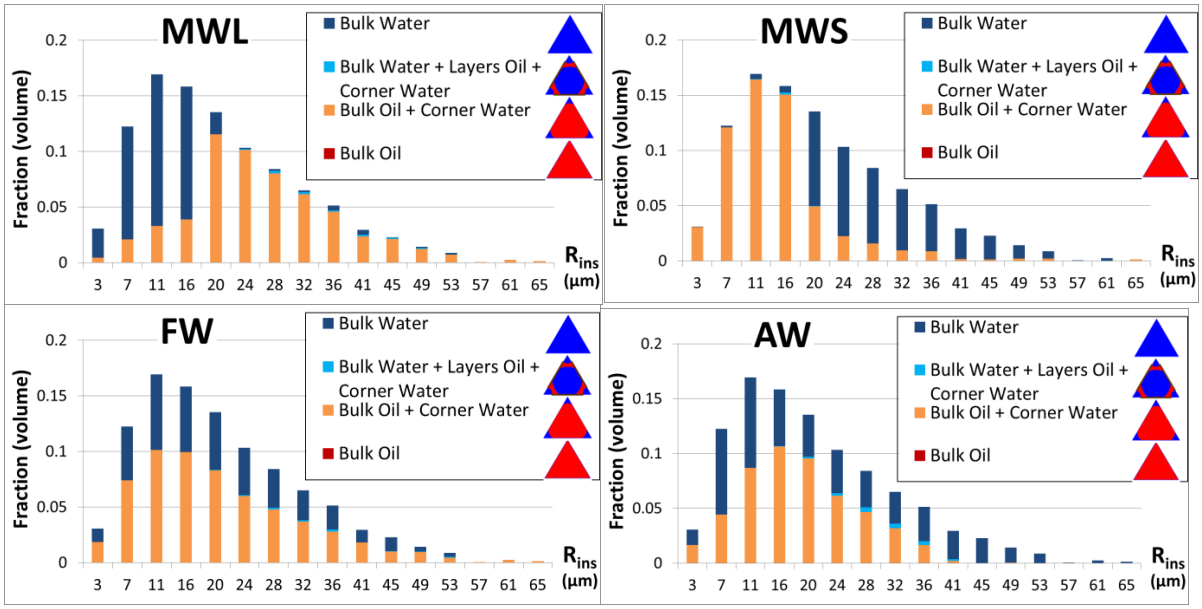

Figure 11: Pore occupancies at the end of the waterflood for the different wettability distributions shown on the pore size distribution for the Berea network at $f_{ow} = 0.5$.

3.1.2.2 Effect of initial water saturation

A sensitivity study to S_{wi} was conducted for the AW distribution. Note that because f_{ow} is defined as a fraction of all pores, the maximum value that it can take is $1 - S_{wi}$, since the remaining fraction S_{wi} is water-filled and water-wet. This explains the different curve endpoints for the different S_{wi} in Figure 12.

Figure 12a shows that at $f_{ow} = 0.5$, with S_{wi} increasing from 0 to 0.1, i.e. strongly decreasing ${P_c}^{max}$ (see Figure 7a), S_{or} slightly increases. This is mainly due to the fact that the oil layer formation is inhibited at relatively low ${P_c}^{max}$. The trend is amplified for higher $f_{ow} = 0.8$, for which the oil layers are more abundant, thus more effective in maintaining the oil connectivity. Further increasing S_{wi} leads to monotonically decreasing S_{or}, as the oil saturation before waterflood, $1 - S_{wi}$, decreases. Nevertheless, the effect of S_{wi} on the S_{or} curves is considered to be small compared to the heterogeneous carbonate case (Section 3.2.3.3).

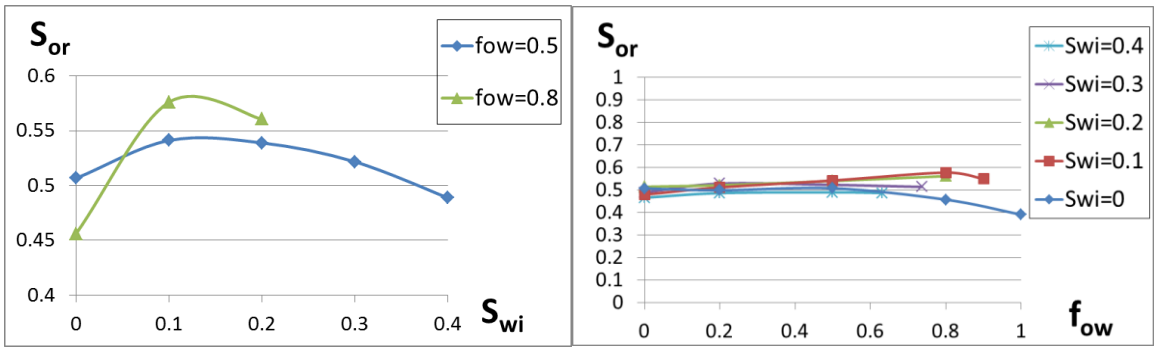

(a) (b)

Figure 12: Waterflood residual oil saturations for the AW distribution in the Berea network as a function of (a) S_{wi} (b) f_{ow}.

3.2. Multiscale Microporous Carbonate

In this section, the input for the two-phase flow model is a heterogeneous network (Figure 13c) constructed from a multiscale dataset for a microporous carbonate, and whose characteristics are summarised in Table 3. The methodology and workflow of the two-scale network generation have been presented by **Jiang et al. (2013)**. First, 3D pore networks were extracted from CT images at two distinct resolutions (fine and coarse scales), which have some overlap in pore sizes. A statistical network generation tool was then used to integrate the two networks into a single pore network (Figure 13). Note that the coarse scale network clearly lacks overall connectivity (Figure 13b), and has only become connected through integration with the well-connected fine scale network (Figure 13a).

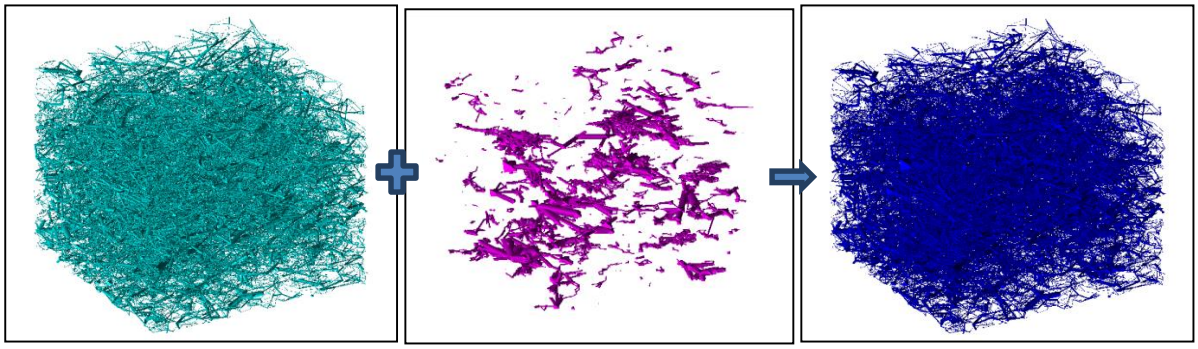

(a) *(b)* *(c)*

Figure 13: (a) Statistically generated fine network, (b) extracted coarse network and (c) resulting integrated two-scale network, derived from a microporous carbonate dataset.

Number of pore elements	*104,138*
Average coordination number	*3.54*
Porosity (%):	*20.38*
Absolute Permeability (mD):	*93.56*

Table 3: Main properties of the carbonate network.

Figure 14 indicates a wide distribution of pore radii in the resulting two-scale network, ranging from 1 to 152 µm, and that micropores ($R_{ins} < 5\mu m$) represent around 18 % of the network volume (corresponding to the first bin in the pore size distribution). Additionally, note that the micropores have a wide range of pore shapes.

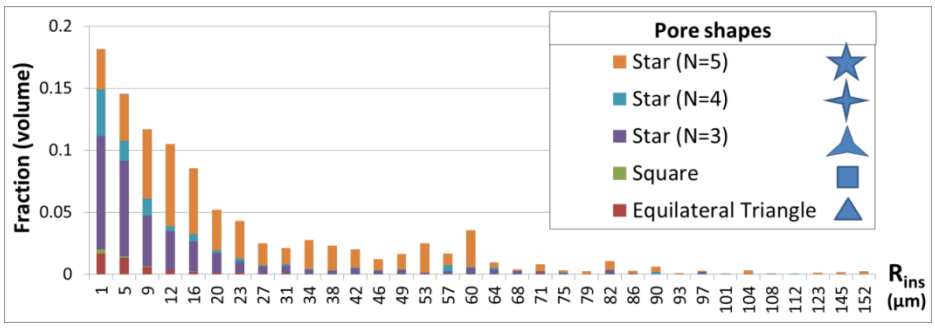

Figure 14: carbonate network pore size (inscribed radius) and shape distributions.

3.2.1. Primary Drainage

As for the Berea network, the primary drainage (PD) process is continued until the irreducible water saturation, approximately $S_{wi} = 0$, is reached at a relatively high $P_c{}^{max} = 50kPa$ (Figure 15), due to the small sizes of the micropores. At $S_{wi} = 0.3$, remaining water resides mainly in the micropores, since their capillary entry pressures are highest (Figure 16). Moreover, as for the Berea network (Figure 8), a small fraction of larger not-yet-accessible pores still retain water. Observe from the oil relative permeability K_r curve (Figure 15b) that oil breakthrough happens at the relatively large water saturation $S_w = 0.86$, as oil first invades a significant fraction of the well-connected fine scale pores. This also explains the rapid drop in K_{rw} for large S_w.

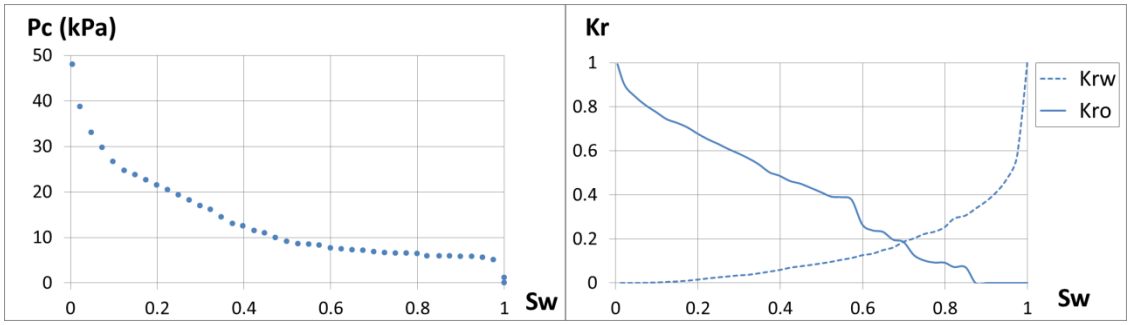

(a) (b)

Figure 15: Primary drainage (a) P_c and (b) K_r curves for the carbonate network.

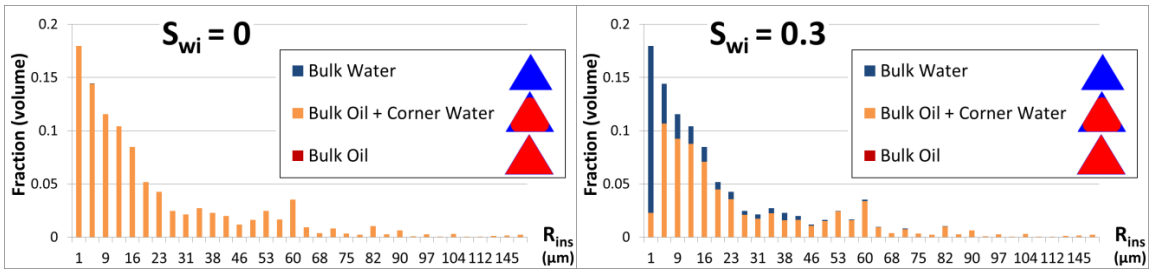

Figure 16: Pore occupancies for the carbonate network shown on the pore size distribution following PD to different S_{wi} values.

3.2.2. Ageing

Following ageing, the resulting wettability distributions within the carbonate network are shown in Figure 17. When comparing the wettability distributions for the carbonate network in Figure 17 with those for the Berea network in Figure 9, it can be seen that the MWL, MWS and FW distributions are (by definition) qualitatively quite similar. The AW distributions are similar as well, but only for the largest pores, as that remain water-wet. However, the striking difference for AW occurs in the smallest pores. Indeed, for the carbonate network, unlike for the Berea, 80% of the micropores are oil-wet, since their small sizes provide sufficient curvature for the water films to break for most of their shapes.

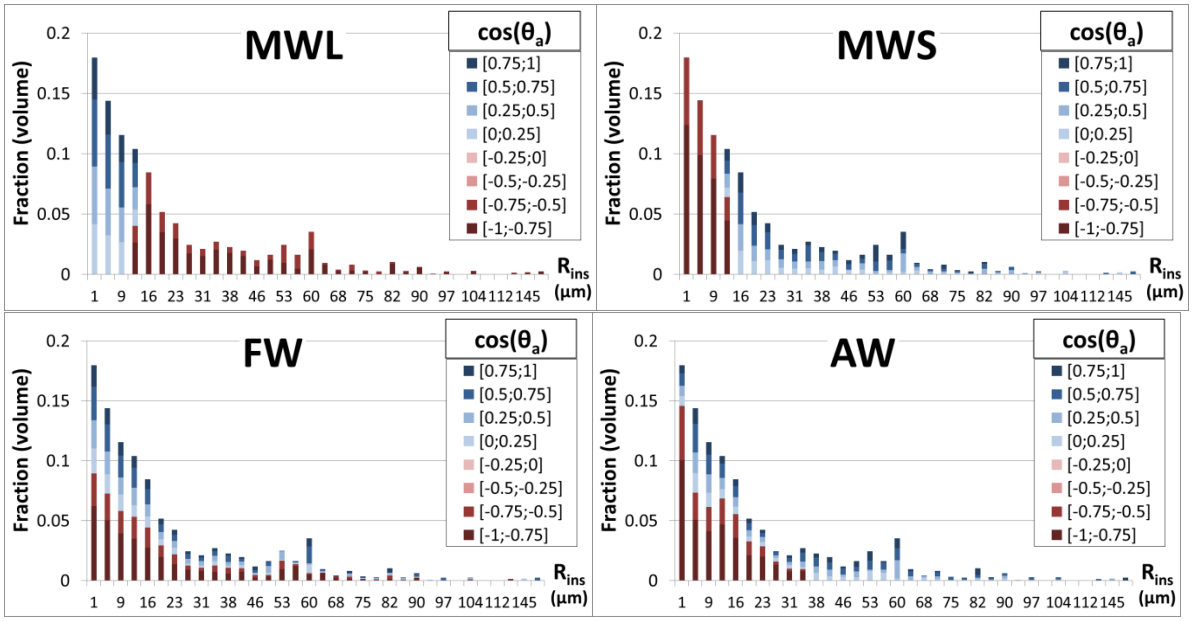

Figure 17: Different wettability distributions shown on the pore size distributions for the carbonate network at $f_{ow} = 0.5$, established after PD for the base case; red: oil-wet, blue: water-wet. Darker blue (resp. red) indicates stronger water- (resp. oil) -wetness.

3.2.3. Waterflood

3.2.3.1 Effect of wettability distribution

The wettability distribution significantly affects the petrophysical properties for the carbonate network (Figure 18). Indeed, the residual oil varies greatly, as S_{or} decreases from 0.75 for MWL to 0.28 for MWS. In addition, P_c curves are found to be dissimilar as a result of the different pore-filling sequences, and there are also corresponding differences in the relative permeability (K_r) curves. The latter is further emphasised by the fractional flow of water, F_w, derived from the K_r curves (Figure 19d), and computed (assuming identical phase viscosities) as

$$F_w = \frac{1}{1+\frac{K_{ro}}{K_{rw}}} \quad (4)$$

F_w appears in the Buckley-Leveret equation when modelling water flooding at the continuum-scale and it shows here that water breakthrough occurs at very different water saturations.

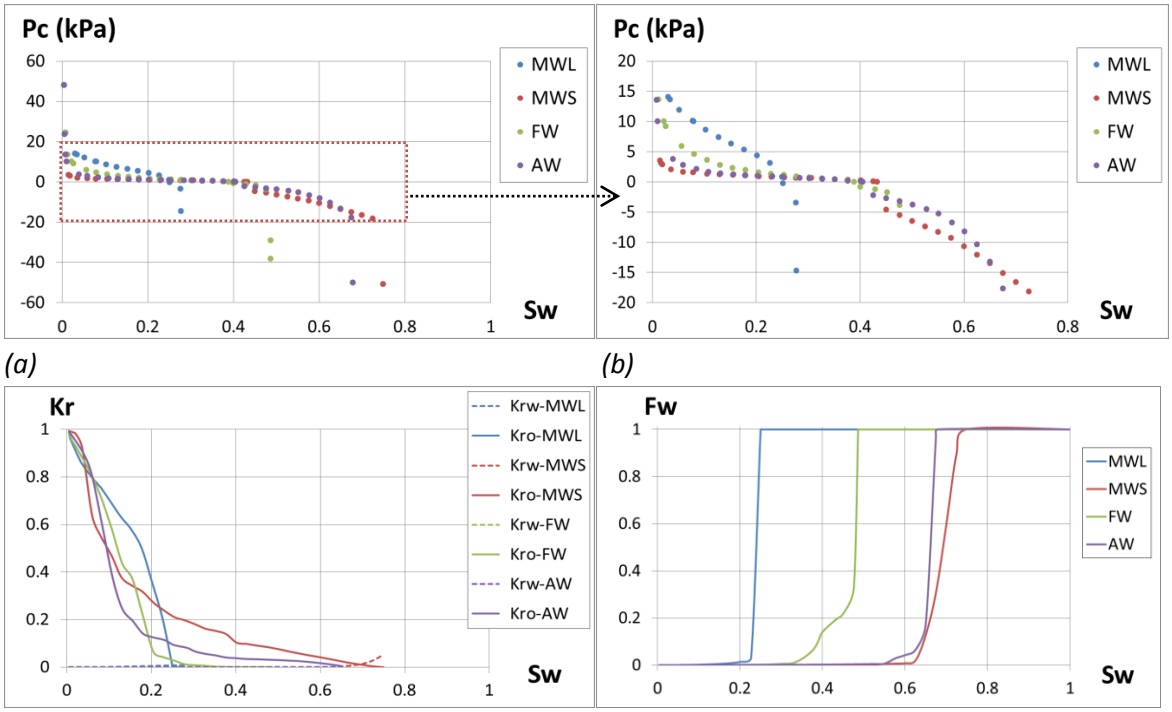

Figure 18: (a) P_c curves, (b) enlarged P_c curves (red box), (c) K_r curves and (d) fractional flow of water, f_w, curves after waterflood for the different wettability distributions at $f_{ow} = 0.5$ for the carbonate network.

The pore occupancies at the end of the waterflood are presented in Figure 19 for all four wettability distributions. Note that, in general, water would start filling water-wet pores (from small to large), then oil-wet pores (from large to small), unless this is prevented by lack of accessibility and trapping. Since the fine scale pores provide the overall connectivity for the disconnected coarse scale pores (Section 3.2), two interesting limiting cases stand out, MWL and MWS.

In the MWL distribution, a fraction of the fine scale pores are water-wet, thus first filled with water. However, these water-filled pores now block the escape of oil from the coarse scale pores, thus leaving much oil trapped in the largest pores, as well as in intermediate-sized pores and some micropores. The capillary pressure curve for this case (see Figures 18a and b), confirms that almost exclusively small, i.e. water-wet, pores are invaded. Hence, trapping in the MWL case is high compared to the other distributions.

Conversely, in the MWS case, water first starts filling the larger water-wet pores. Note that all pores have corner wetting films (see Figure 16a); therefore all pores are accessible to the invading water, even though the coarse scale network is disconnected. Water invasion then continues in the smaller oil-wet pores. The corresponding jump in invaded pore size is translated into a large drop in P_c over a small saturation range in the capillary pressure curve (Figure 18b). By leaving the micropores to be filled at the end of the process, MWS has the lowest trapping of all wettability distributions.

The pore occupancy for the AW distribution (Figure 19d) is similar to that for MWS, in contrast to the occupancies for the Berea network, while the occupancy for FW exhibits behaviour intermediate to MWS and MWL.

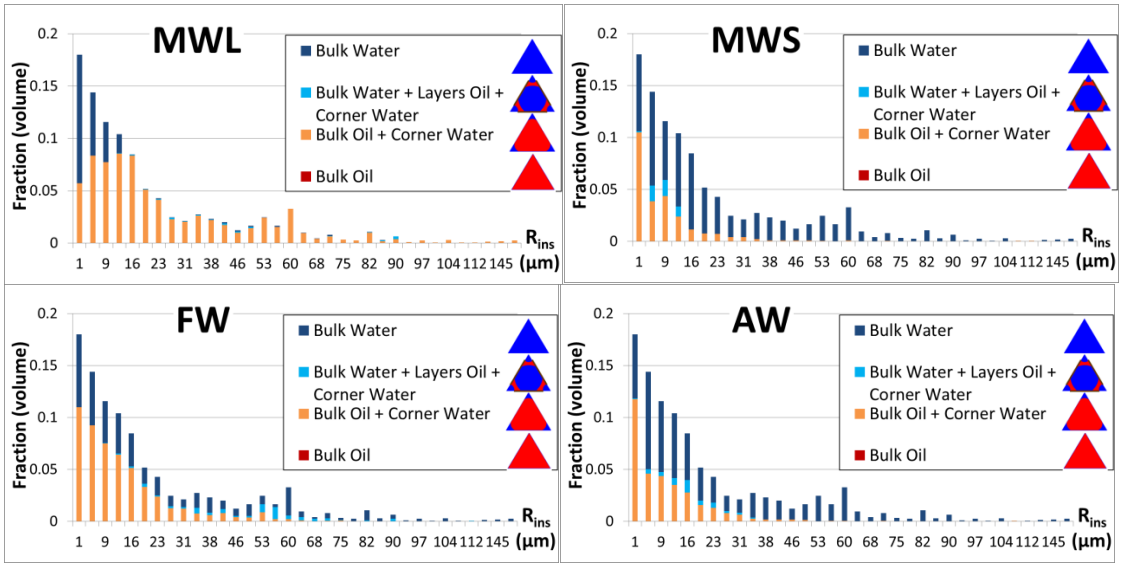

Figure 19: Pore occupancies at the end of the waterflood for the different wettability distributions shown on the pore size distribution for the carbonate network at $f_{ow} = 0.5$.

3.2.3.2 Effect of oil-wet fraction

We now consider the AW distribution, and study the impact of changing the fraction of oil-wet pores, f_{ow}, on the petrophysical properties. Considering the residual oil saturation, the trend is visibly monotonic, as S_{or} decreases with f_{ow} (Figure 20). We note as well that the switch from fully water-wet ($f_{ow} = 0$) to less water-wet ($f_{ow} = 0.2$) leads to a large reduction in S_{or}, as a fraction of the micropores become oil-wet. However, further changing to fully oil-wet has a relatively small effect. The impact of the presence of oil layers on S_{or} shown in Figure 21b is similar to that seen in the Berea network (Figure 10b). With regard to P_c curves, they are lower for larger fractions of oil-wet pores, as expected.

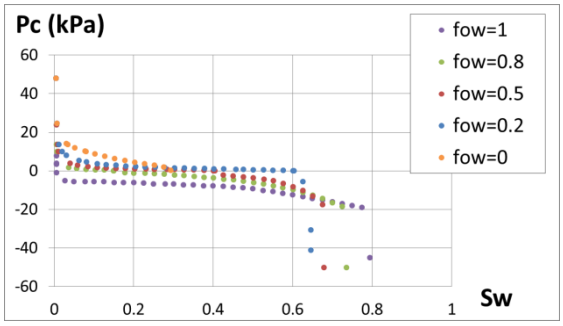

Figure 20: P_c curves after waterflood for different oil-wet fractions for the carbonate network.

The results of this sensitivity study are summarised in Figure 21a, where both the wettability distribution and f_{ow} are varied. Unlike for the Berea sandstone (see Figure 10a), the S_{or} values are very different for the various wettability distributions in this microporous carbonate. The MWS and MWL distributions clearly form the limiting boundaries for the residual oil saturations. Indeed, the

best recovery is exhibited by MWS, while MWL shows the worst recovery. On the other hand, recoveries for the developed AW distribution and the FW distribution lie between the two extreme cases, but they still differ significantly from each other.

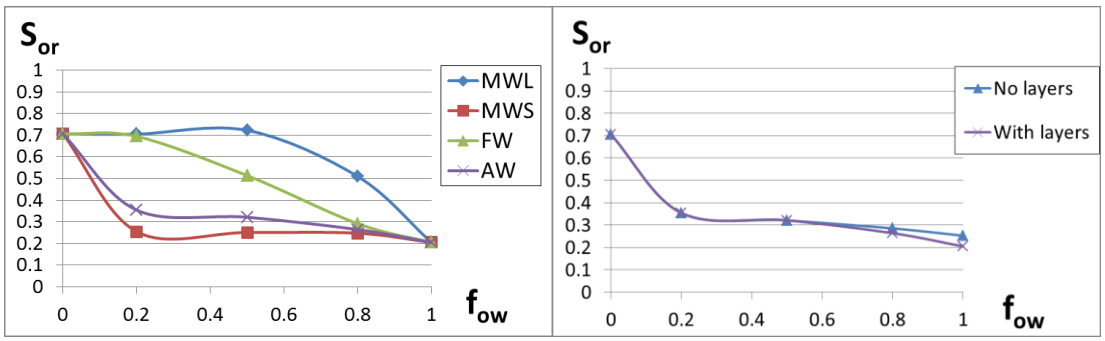

(a) (b)

Figure 21: Waterflood residual oil saturations as a function of oil-wet fractions for the carbonate network (a) for the different wettability distributions, and (b) for the AW distribution, with and without oil layers.

3.2.3.3. Effect of initial water saturation

First, note that since we are lacking real S_{wi} (or $P_c^{\max}$) data, zero initial water saturation, $S_{wi} = 0$, was chosen as a base case to highlight the impact that the wettability of micropores has on recovery. In fact, oil presence in micropores has been reported in many real carbonate rocks, especially towards the top of the oil column. This could happen if the reservoir has a sufficiently large oil column such that a high capillary pressure is reached in the upper oil column, or if some pores have somehow undergone a reduction in size (e.g. by means of cementation or dissolution) or in wettability (e.g. due to polar species in the oil) over geological time.

S_{or} curves are plotted in Figure 22 for different S_{wi} values. The trends are similar to those observed in the Berea network (Figure 12) but the variations and the differences between the curves for varying f_{ow} are much larger. Actually, while increasing S_{wi}, added to the fact that fewer oil layers form, more water is retained in the micropores at the start of the waterflood, which in turn blocks the escape of oil in the bigger pores due to the particular (reduced) connectivity of the carbonate network.

To examine the structure of the residual oil (**Ryazanov et al., 2014**), we show in Figure 23 the pore occupancies at the end of the water flood for different S_{wi} values at $f_{ow} = 0.5$. Since the initial water resides mostly in the micropores (see Figure 16), the nature of the residual oil changes with higher S_{wi}, as oil is increasingly trapped in intermediate-sized pores and less so in micropores. Besides, as previously stated in Section 3.1.2.2, oil layers are less likely to develop at lower $\mathrm{P_c}^{\max}$, i.e. at higher S_{wi}.

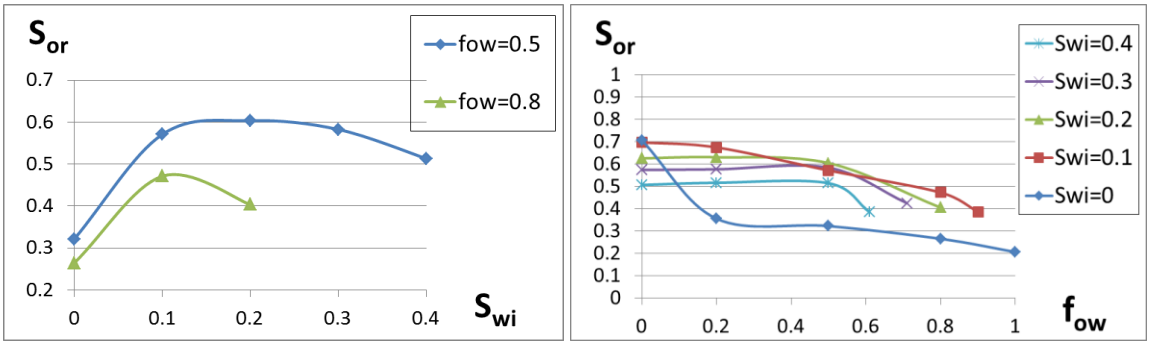

Figure 22: Waterflood residual oil saturation for the AW distribution in the carbonate network as a function of (a) S_{wi} (b) f_{ow}.

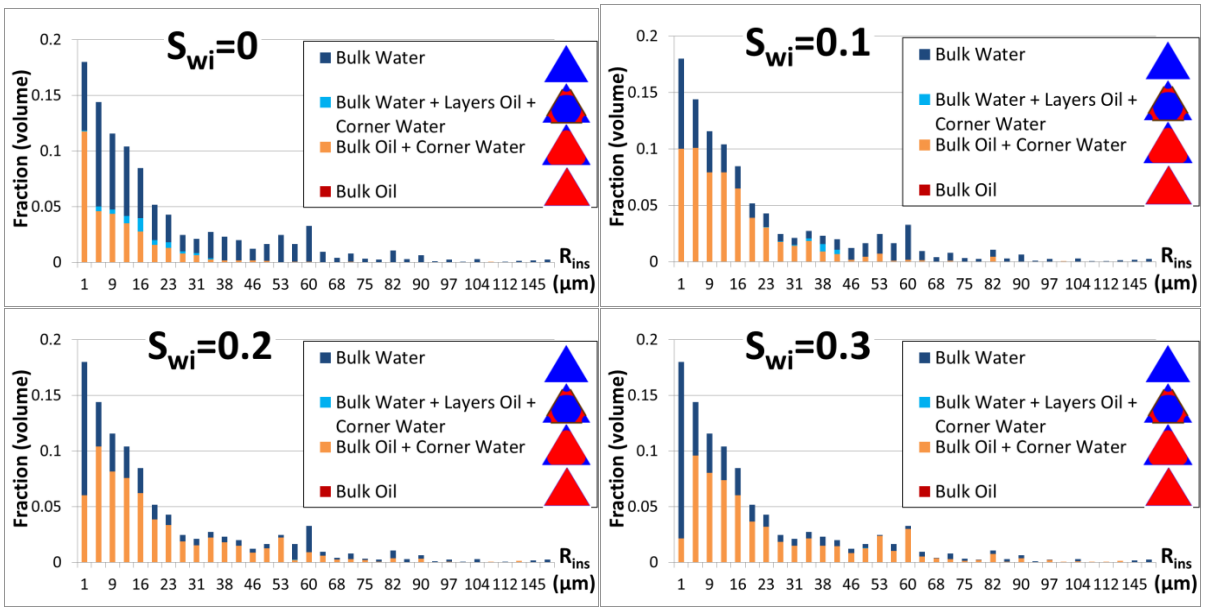

Figure 23: Pore occupancies at the end of the waterflood for different S_{wi} values shown on the pore size distribution for the carbonate network at $f_{ow} = 0.5$.

Note that by keeping the oil-wet fraction constant ($f_{ow} = 0.5$) and increasing S_{wi} (decreasing P_c^{max}) (Figure 22), the corresponding Π_{crit} value is decreasing. This may not be realistic since Π_{crit} is assumed to be an intrinsic property of the rock mineral and water film sub-system. Indeed, the "right" way would be to keep Π_{crit} constant, increase S_{wi}, and consequently obtain a lower f_{ow}. However, this was not feasible in our model because f_{ow} is highly sensitive to S_{wi}. This is mainly due to the nature of the primary drainage curve at high oil saturations. Indeed, high capillary pressures need to be overcome to displace small amounts of water. For instance, if Π_{crit} were chosen such that $f_{ow} = 0.5$ for $S_{\mathrm{wi}} = 0$ (for which $\mathrm{P_c}^{\max} = 48kPa$), changing S_{wi} to 0.1 would reduce P_c^{max} to 27*kPa*. The latter value would be below the critical capillary pressure P_c^* of all pores, keeping all water films intact, thus $f_{ow} = 0$. The corollary is that if Π_{crit} were chosen such that a fraction of pores becomes oil-wet for lower values of P_c^{max}, i.e. for non-zero S_{wi}, f_{ow} would always be close to 1 for $S_{\mathrm{wi}} = 0$.

4. Conclusions

We developed a physically-based wettability alteration scenario, dependent on both pore size and shape, which incorporates a plausible view of the wetting change mechanism. The scenario qualitatively reproduced a pattern of wettability observed in microporous carbonates through high-resolution imaging, where anhedral (curved, rough and poorly formed) faces become preferentially oil-wet. We implemented the scenario in a two-phase quasi-static pore network model which involves a variety of pore shapes. We considered as input two pore networks with very different levels of complexity in their pore structure, (a) a fairly homogeneous connected Berea sandstone network with a relatively narrow range of pore sizes, and (b) a heterogeneous two-scale carbonate network whose coarse scale pores were not connected, but where the fine scale pores provided overall connectivity to the network. We considered the widest possible range of wettability distributions, including the Altered-Wet (AW) distribution, based on the newly developed scenario, along with the commonly used MWL, MWS and FW distributions. This resulted in a correspondingly wide range of outcomes in terms of pore occupancies, P_c and K_r curves and S_{or} values.

During primary drainage, we showed that, at non-zero S_{wi}, most of the connate water was naturally found in the smallest pores, as well as in a few larger not-yet-accessible pores. After ageing was carried out, the AW distribution resulted in the largest pores being water-wet, as their large size prevented them from having sufficient curvature for the water film to collapse. Conversely, owing to their tiny size, most of the carbonate network's micropores were found to be oil-wet, provided that they were invaded by oil during primary drainage. Yet, the AW distribution was still distinct from the MWS, as well as from any of the other common wettability distributions. Following waterflooding, we showed from the pore occupancies that the specific wettability distribution affects the structure of the residual oil. In addition, wettability proved to have some effect on the residual oil saturation (S_{or}) for the Berea network, but it had a much larger impact for the multiscale carbonate network. Indeed, since the connectivity of this network is mainly driven by pore size, the MWS and MWL distributions formed limiting cases for the S_{or} values, with the recoveries for the AW and FW distributions lying between these two extremes. The MWL case exhibited by far the lowest oil recovery since the first-filled water-wet micropores blocked the escape of oil from the larger pores. Conversely, the MWS distribution showed the best recovery as the oil-wet micropores are left to be water-filled at the end of the waterflood. In addition, the relative permeability curves for the carbonate network were very sensitive to the chosen wettability distribution. This was emphasised by the corresponding fractional flow curves, which showed very different water breakthrough saturations. Furthermore, we demonstrated that oil layers did indeed allow oil to drain to lower S_{or}, but only at a sufficiently high f_{ow}. Moreover, by increasing S_{wi}, we first observed higher S_{or}, due to fewer oil layers being formed, and then lower S_{or} because of a decreasing oil fraction before waterflood. We proved that these trends are amplified at higher f_{ow} values where more oil layers form, as well as in the carbonate network where the effect of the network's particular connectivity contributes notably. Indeed, the increased volumes of connate water left behind in the micropores consequently trap the oil in the larger pores.

Wettability has long played the role of a sort of "tuning parameter" in simulations, although in actual calculations it is the consequent petrophysical function (P_c and K_{ro}) that is actually used or varied; no "number for wettability" appears in any oil displacement calculation. However, there is strong evidence from pore network modelling (supported again by the results presented here) that

the actual assumptions on the wetting distribution do strongly influence these petrophysical functions as well as the S_{or} value. Thus, if we had some prior knowledge of these wetting patterns, then we might be able to forward model the petrophysical functions. Working petrophysicists and core analysts in the oil industry do have views on the physical forms of these wetting patterns. Therefore, we suggest building up "Type diagrams" of wetting patterns in carbonate rocks by consideration of the possible mechanisms involved, such as those incorporated in the developed AW model. The patterns generated can then be presented to petrophysics experts who will recognise the most likely physically realistic patterns. This approach is used in other industries and is known as expert elicitation **(Curtis and Wood, 2005)**. At best such a scenario might generate in a systematic manner prior probabilities of certain wetting patterns for realistic carbonates. We believe that this is the only way that a combination of flow physics, forward modelling and industry expertise/knowledge can be combined to make some advances in modelling complex mixed-wet systems at the pore level.

Acknowledgements

The authors would like to thank the members of the ITF consortium, DONG energy, Wintershall, BG Group and Chevron, for funding this work.

References

Al-Yousef, H.Y., Lichaa, P.M., Al-Kaabi, A.U., Alpustun, H.: Wettability Evaluation of a Carbonate Reservoir Rock from Core to Pore Level. Paper presented at the Society of Petroleum Engineers, Middle East Oil Show, Bahrain, 11-14 March 1995

Amott, E.: Observations Relating to the Wettability of Porous Rock. In, vol. 216. pp. 156-162. Petroleum Transactions, AIME, (1959)

Blunt, M.J.: Effects of Heterogeneity and Wetting on Relative Permeability Using Pore Level Modeling. SPE Journal **2**(01), 70 - 87 (1997a). doi:10.2118/36762-PA

Blunt, M.J.: Pore Level Modeling of the Effects of Wettability. SPE Journal **2**(04), 494 - 510 (1997b). doi:10.2118/38435-PA

Blunt, M.J.: Physically-based network modeling of multiphase flow in intermediate-wet porous media. Journal of Petroleum Science and Engineering **20**(3-4), 117-125 (1998). doi:Doi 10.1016/S0920-4105(98)00010-2

Cantrell, D.L., Hagerty, R.M.: Microporosity in Arab Formation Carbonates, Saudi Arabia. GeoArabia **4**, 129 - 154 (1999)

Clerke, E.A.: Permeability, Relative Permeability, Microscopic Displacement Efficiency and Pore Geometry of M_1 Bimodal Pore Systems in Arab-D Limestone. SPE Journal **14**(03), 524 - 531 (2009). doi:10.2118/105259-PA

Clerke, E.A., Aramco, S., Allen, D.F., Crary, S.C., Srivastava, A., Ramamoorthy, R., Saldungaray, P., Savundararaj, P., Heliot, D., Goswami, J., Bordakov, G.: Wireline Spectral Porosity Analysis of the Arab Limestone—From Rosetta Stone to Cipher. Paper presented at the SPWLA 55th Annual Logging Symposium, Abu Dhabi, United Arab Emirates, 18-22 May, 2014

Curtis, A., Wood, R.: Optimal elicitation of probabilistic information from experts. In: Wood, R. (ed.) Geological Prior Information. Geological Society London, (2005)

Dixit, A.B., Buckley, J.S., McDougall, S.R., Sorbie, K.S.: Empirical Measures of Wettability in Porous Media and the Relationship between Them Derived From Pore-Scale Modelling. Transport in Porous Media **40**(1), 27-54 (2000). doi:10.1023/A:1006687829177

568 Dixit, A.B., McDougall, S.R., Sorbie, K.S., Buckley, J.S.: Pore-Scale Modeling of Wettability Effects and
569 Their Influence on Oil Recovery. SPE Reservoir Evaluation & Engineering **2**(01), 25 - 36
570 (1999). doi:10.2118/54454-PA
571 Dodd, N., Marathe, R., Middleton, J., Fogden, A., Carnerup, A., Knackstedt, M., Mogensen, K.,
572 Marquez, X., Frank, S., Bounoua, N., Noman, R.: Pore-Scale Imaging of Oil and Wettability in
573 Native-State, Mixed-Wet Reservoir Carbonates. Paper presented at the International
574 Petroleum Technology Conference, Doha, Qatar, 19-22 January, 2014
575 Donaldson, E.C., Thomas, R.D., Lorenz, P.B.: Wettability Determination and Its Effect on Recovery
576 Efficiency. Society of Petroleum Engineers Journal **9**(1), 13 - 20 (1969). doi:10.2118/2338-PA
577 Fassi-Fihri, O., Robin, M., Rosenberg, E.: Wettability Studies at the Pore Level: A New Approach by
578 the Use of Cryo-Scanning Electron Microscopy. SPE Formation Evaluation **10**(01), 11 - 19
579 (1995). doi:10.2118/22596-PA
580 Frette, O.I., Virnovsky, G., Hildebrand-Habel, T.: Modelling the stability of thin water films using SEM
581 images. Paper presented at the EUROPEC/EAGE Conference and Exhibition, Amsterdam, The
582 Netherlands, 8-11 June, 2009
583 Fung, L.S.K., Middya, U., Dogru, A.H.: Numerical Simulation of Fractured Carbonate Reservoirs with
584 the M_1 Bimodal Pore System. Paper presented at the SPE Reservoir Simulation Symposium,
585 The Woodlands, Texas, 21-23 February, 2011
586 Hamon, G.: Field-Wide Variations of Wettability. Paper presented at the Society of Petroleum
587 Engineers, 2000
588 Helland, J.O., Ryazanov, A., Van Dijke, M.I.J.: Characterization of pore shapes for pore network
589 models. Paper presented at the ECMOR XI: 11th European Conference on the Mathematics
590 of Oil recovery, Bergen, Norway, 8 - 11 Sept, 2008
591 Hirasaki, G.J.: Wettability: Fundamentals and Surface Forces. SPE Formation Evaluation **6**(02), 217 -
592 226 (1991). doi:10.2118/17367-PA
593 Jackson, M.D., Valvatne, P.H., Blunt, M.J.: Prediction of wettability variation and its impact on flow
594 using pore- to reservoir-scale simulations. Journal of Petroleum Science and Engineering
595 **39**(3-4), 231-246 (2003). doi:10.1016/s0920-4105(03)00065-2
596 Jadhunandan, P.P., Morrow, N.R.: Effect of Wettability on Waterflood Recovery for Crude-
597 Oil/Brine/Rock Systems. SPE Reservoir Engineering **10**(01), 40 - 46 (1995).
598 doi:10.2118/22597-PA
599 Jiang, Z., van Dijke, M.I.J., Sorbie, K.S., Couples, G.D.: Representation of multiscale heterogeneity via
600 multiscale pore networks. Water Resources Research **49**(9), 5437-5449 (2013).
601 doi:10.1002/wrcr.20304
602 Jiang, Z., Wu, K., Couples, G., van Dijke, M.I.J., Sorbie, K.S., Ma, J.: Efficient extraction of networks
603 from three-dimensional porous media. Water Resources Research **43**(12), n/a-n/a (2007).
604 doi:10.1029/2006wr005780
605 Joekar-Niasar, V., Prodanović, M., Wildenschild, D., Hassanizadeh, S.M.: Network model
606 investigation of interfacial area, capillary pressure and saturation relationships in granular
607 porous media. Water Resources Research **46**(6), n/a-n/a (2010). doi:10.1029/2009wr008585
608 Knackstedt, M.A., Pinczewski, W.V., Fogden, A., Senden, T.: Improved characterization of EOR
609 processes in 3D. Characterizing mineralogy, wettability and residual fluid phases at the pore
610 scale. Paper presented at the SPE Enhanced Oil Recovery Conference, Kuala Lumpur,
611 Malaysia, 19-21 July, 2011
612 Kovscek, A.R., Wong, H., Radke, C.J.: A pore-level scenario for the development of mixed wettability
613 in oil reservoirs. AIChE Journal **39**(6), 1072-1085 (1993). doi:10.1002/aic.690390616
614 Lichaa, P.M., Alpustun, H., Abdul, J.H., Nofal, W.A., Fuseni, A.B.: Wettability Evaluation of a
615 Carbonate Reservoir Rock. Advances in Core Evaluation III, Reservoir Management **327**
616 (1993)
617 Marathe, R., Turner, M.L., Fogden, A.: Pore-Scale Distribution of Crude Oil Wettability in Carbonate
618 Rocks. Energy & Fuels **26**(10), 6268-6281 (2012). doi:10.1021/ef301088j

McDougall, S.R., Dixit, A.B., Sorbie, K.S.: Network analogues of wettability at the pore scale. Geological Society, London, Special Publications **122**(1), 19-35 (1997)
McDougall, S.R., Sorbie, K.S.: The Impact of Wettability on Waterflooding: Pore-Scale Simulation. SPE Reservoir Engineering **10**(03), 208 - 213 (1995). doi:10.2118/25271-PA
Okasha, T.M., Funk, J.J., Rashidi, H.N.: Fifty Years of Wettability Measurements in the Arab-D Carbonate Reservoir. Paper presented at the SPE Middle East Oil and Gas Show and Conference, Kingdom of Bahrain, 11-14 March, 2007
Oren, P.E., Bakke, S., Arntzen, O.J.: Extending Predictive Capabilities to Network Models. SPE Journal **3**(04), 324 - 336 (1998). doi:10.2118/52052-PA
Patzek, T.W.: Verification of a Complete Pore Network Simulator of Drainage and Imbibition. SPE Journal **6**(02), 144 - 156 (2001). doi:10.2118/71310-PA
Ryazanov, A.V., Dijke, M.I.J., Sorbie, K.S.: Two-Phase Pore-Network Modelling: Existence of Oil Layers During Water Invasion. Transport in Porous Media **80**(1), 79-99 (2009). doi:10.1007/s11242-009-9345-x
Ryazanov, A.V., Sorbie, K.S., van Dijke, M.I.J.: Structure of residual oil as a function of wettability using pore-network modelling. Advances in Water Resources **63**, 11-21 (2014). doi:10.1016/j.advwatres.2013.09.012
Salathiel, R.A.: Oil Recovery by Surface Film Drainage In Mixed-Wettability Rocks. Journal of Petroleum Technology **23**(10) (1973). doi:10.2118/4104-PA
Sharma, M.M., Wunderlich, R.W.: The alteration of rock properties due to interactions with drilling-fluid components. Journal of Petroleum Science and Engineering **1**(2), 127-143 (1987). doi:http://dx.doi.org/10.1016/0920-4105(87)90004-0
Skauge, A., Sørvik, A., Vik, B., Spildo, K.: Effect of wettability on oil recovery from carbonate material representing different pore classes. Paper presented at the International Symposium of the Society of Core Analysts, Trondheim, Norway, 2006
Skauge, A., Spildo, K., Høiland, L., Vik, B.: Theoretical and experimental evidence of different wettability classes. Journal of Petroleum Science and Engineering **57**(3-4), 321-333 (2007). doi:10.1016/j.petrol.2006.11.003
Valvatne, P.H., Blunt, M.J.: Predictive pore-scale modeling of two-phase flow in mixed wet media. Water Resources Research **40**(7), n/a-n/a (2004). doi:10.1029/2003wr002627
van Dijke, M.I., Sorbie, K.S.: Existence of fluid layers in the corners of a capillary with non-uniform wettability. Journal of colloid and interface science **293**(2), 455-463 (2006). doi:10.1016/j.jcis.2005.06.059
Zhao, X., Blunt, M.J., Yao, J.: Pore-scale modeling: Effects of wettability on waterflood oil recovery. Journal of Petroleum Science and Engineering **71**(3-4), 169-178 (2010). doi:10.1016/j.petrol.2010.01.011